1 **Drawdown of Atmospheric pCO$_2$ via Variable Particle Flux Stoichiometry in the Ocean Twilight Zone**

2 Tatsuro Tanioka[1,2 *], Katsumi Matsumoto[1], and Michael W. Lomas[3]

3 [1] Department of Earth & Environmental Sciences, University of Minnesota, Minneapolis, MN, USA
4 [2] Department of Earth System Science, University of California Irvine, Irvine, CA, USA
5 [3] Bigelow Laboratory for Ocean Sciences, East Boothbay, ME, USA

6 *Correspondence to*: Tatsuro Tanioka (tatsurt@uci.edu)

7

8 **Key Points:**

9 • Global particle flux data suggests a systematic increase in carbon (C) to phosphorus (P) flux
10 stoichiometry in the ocean twilight zone.

11 • Increase in the C:P export flux ratio through the twilight zone can substantially increase atmospheric
12 *pCO$_2$* drawdown.

13 • Further studies are required to elucidate mechanisms leading to spatiotemporal C:P export flux
14 variability in the twilight zone.

15

16

17

18

19

20

21

22

23

24

25

26

27

28

Abstract

The strength of the biological soft tissue pump in the ocean critically depends on how much
organic carbon is produced via photosynthesis and how efficiently the carbon is transferred to
the ocean interior. For a given amount of limiting nutrient, phosphate, soft tissue pump would
be strengthened if the carbon (C) to phosphorus (P) ratio of sinking organic matter increases
as the remineralization length scale of C increases. Here, we present a new data compilation
of particle flux stoichiometry and show that C:P of sinking particulate organic matter (POM)
in the ocean twilight zone on average is likely to be higher than the C:P ratio of surface
suspended POM. We further demonstrate using a physics-biology coupled global ocean
model combined with a theory from first principles that an increase in C:P export flux ratio in
the ocean's twilight zone can lead to a considerable drawdown of atmospheric pCO_2.

Plain Language Summary

The ocean's twilight zone, located below the ocean's sunlit zone, is a region where many
critical biogeochemical processes occur but are not well characterized. Most notably, this is
the zone where microbes and animals consume organic matter produced by primary
producers in the surface ocean. How efficiently this organic matter is degraded exerts
essential controls on atmospheric carbon dioxide levels and energy transfer in the marine
food web. Here we show using a new global data compilation that organic carbon and
phosphorus particles are degraded at different rates. This leads to a considerable change in
carbon to phosphorus ratio at depth. We incorporate this variability into the 3D ocean model
to show that such change can substantially increase the ocean's ability to absorb carbon
dioxide from the atmosphere. The study ultimately highlights the need to accurately
characterize the ocean's role in climate change by studying the particle dynamics in the
twilight zone.

1. Introduction

The biological carbon pump is one of the critical mechanisms whereby marine phytoplankton
convert inorganic carbon into organic carbon via photosynthesis, and that carbon is
subsequently transported into the ocean interior (Sigman & Boyle, 2000). The conventional
thinking is that oceanic carbon storage due to the biological carbon pump is proportional to
the total inventory of phosphate in the interior ocean that arrived through the biological
"regenerated" pathway (Ito & Follows, 2005; Marinov, Gnanadesikan, et al., 2008). This
hypothesis assumes a fixed C:P stoichiometry, where carbon transfer efficiency into the
ocean interior is tightly coupled to the transfer of phosphate from surface to depth. Under this
framework, an increase in POM transfer efficiency and associated drawdown on atmospheric

64 *pCO2* will rapidly deplete surface nutrients, most notably in the North Atlantic and the
65 Southern Ocean regions, where most deep water is formed (Sarmiento & Toggweiler, 1984).
66
67 Another school of thought proposes that the biological carbon pump can be strengthened if
68 the C:P ratio of sinking POM increases with depth (Broecker, 1982a, 1982b; Knauer et al.,
69 1979; Menzel & Ryther, 1964). This strengthening can happen if the remineralization length
70 scale of particulate organic carbon (POC) is longer than that of particulate organic
71 phosphorus (POP) such that C:P of the sinking POM exceeds C:P of upward inorganic flux
72 (Christian et al., 1997). The seminal study by Menzel and Ryther (1964) demonstrated by
73 sampling POM in the mesopelagic region of the Western North Atlantic that particulate
74 phosphorus is remineralized more quickly than particulate carbon or nitrogen. Subsequent
75 studies based on sediment traps and hydrographic studies have supported this theory (Knauer
76 et al., 1979; J. H. Martin et al., 1987; Minster & Boulahdid, 1987). Furthermore, a recent
77 inverse model study (Teng et al., 2014) argues that depth-dependent changes in C:P of
78 sinking POM can better explain observed inorganic carbon and phosphate distributions than
79 the model with fixed a C:P.
80
81 Here, we provide new lines of evidence for linking vertical variability in the C:P ratio of
82 sinking POM in the twilight zone to carbon storage by using a compilation of recently
83 published data and the time-series data from the Bermuda Atlantic Time-series Study (BATS).
84 We then use a global ocean biogeochemistry model, combined with a theory derived from
85 first principles, to illustrate that increases in the twilight zone C:P ratio could substantially
86 strengthen the ocean biological carbon pump and drawdown of atmospheric CO_2. Previous
87 modeling studies explored the impacts of remineralization length of particulate organic
88 matter on atmospheric *pCO2,* assuming fixed Redfield C:P stoichiometry throughout the
89 entire water column (Kwon et al., 2009; Lauderdale & Cael, 2021; Matsumoto, 2007). The
90 novelty of our 3D modeling study is that it investigates the effects of C:P changes both at the
91 surface and in the subsurface ocean that also involve stoichiometric interaction between
92 phytoplankton and zooplankton.

93 **2. Methods**

94 **2.1 Data compilation of sinking POM**
95 We compiled a new set of data on POC and POP export fluxes based on previous
96 compilations by Antia (2005), Faul et al. (2005), and Paytan et al. (2003) to gather POC and
97 POP sedimentary flux data that have been collected simultaneously. We have limited our
98 analyses to open ocean samples and excluded coastal samples, and samples from the
99 Southern Ocean as these sites are influenced mainly by resuspended or advected P (Faul et al.,

100 2005). Despite a wide range in sample treatment protocols, consistent trends across data
101 indicate that the trends are not artifacts of sample processing or storage after collection (Faul
102 et al., 2005).
103
104 We also included in our new data compilation several studies that were not included in the
105 previous compilations (Benitez-Nelson et al., 2007; Engel et al., 2017; Grabowski et al.,
106 2019; Karl et al., 2012; Lamborg et al., 2008; Lomas et al., 2010). As a quality control, we
107 only include studies published after 2005 that report latitude and longitude information, and
108 we took the average over the non-overlapping periods if multiple samples are taken from the
109 same latitude and longitude. For brevity, we use the term PP (particulate phosphorus) to
110 describe observed particulate phosphorus fluxes that do not separate particulate inorganic
111 components from organic components. In addition, we limit our study to the samples below
112 the epipelagic zone, operationally defined here as 100 m. Finally, for stations ALOHA and
113 BATS, where multiple studies report sedimentary flux values, we selected the study by
114 Grabowski et al. (2019) and Lomas et al. (2010) to represent the mean values for ALOHA
115 and BATS, respectively. Selection processes based on the above criteria led to a total of 54
116 C:P flux ratio measurements (Table S1).
117
118 We note that of the total 54 measurements, 26 are collected by surface-tethered sediment
119 traps, 25 by moored sediment traps, and 3 by neutrally buoyant free-drifting sediment traps
120 (Table S1). All the surface-tethered samples are from the twilight zone (100 – 1000 m), and
121 the majority of the moored sediment traps are from the deep ocean (> 1000 m). As the local
122 hydrodynamic conditions, degree of solubilization, and the existence of zooplankton
123 swimmers will impact collection bias differently for each sample (Antia, 2005; Buesseler et
124 al., 2007), we report average values over the large geographic and the depth range to provide
125 a broad picture of how C:P flux ratio changes with depth. Oceanographic regions (boundaries
126 shown in Figure 1a) are based on the 0.3 mmol m^{-3} contour of the annually averaged PO_4
127 concentration from World Ocean Atlas 2018 (Garcia et al., 2018).
128
129 In addition to the time-averaged particle flux measurements, we present the continuous
130 sedimentary flux timeseries measurements of POC and PP fluxes from BATS (31° 40' N
131 064°10'W), collected from 2006 to 2019 at three different depths (150, 200, and 300 m).
132 Using this data, we computed the Martin b exponent ($F(z) \propto (z/z_0)^{-b}$) for POC and PP
133 separately for each time point using 150 m as a reference depth z_0. POC and PP sedimentary
134 particle flux from the BATS station were measured using the standard method previously
135 described (Lomas et al., 2010) and are publicly available (http://bats.bios.edu; last access
136 April 23, 2021). All statistical analyses were conducted in R version 4.0.4 (R Core Team,
137 2021).

138
2.2 Ocean Biogeochemical Model
2.2.1 General Overview
We conducted all numerical simulations by applying the transport matrix model (TMM)
(Khatiwala, 2007; Khatiwala et al., 2005) as an efficient offline method to simulate the 3D
transport of tracers in the global ocean. The Transport Matrices (TMs) used in this study are
derived from the circulation of the Estimating the Circulation and Climate of the Ocean
(ECCO) project, with a horizontal resolution of 1° by 1° and 23 levels in the vertical
(Stammer et al., 2004). ECCO circulation field is optimized to best fit hydrographic and
remote sensing observations as well as the mean age of water parcels constrained by transient
tracers (radiocarbon and chlorofluorocarbons, CFCs) (Khatiwala et al., 2012).

TMM circulation field is coupled to Model of Oceanic Pelagic Stoichiometry (MOPS), a
simple NPZD model with nine default prognostic variables: phosphate, nitrate, dissolved
inorganic carbon, alkalinity, oxygen, dissolved organic phosphorus, detritus, a single class of
phytoplankton, and a single class of zooplankton (Kriest & Oschlies, 2015). In the original
MOPS, the central currency of the model is phosphorus and assumes a fixed stoichiometric
ratio of $C:N:P:-O_2 = 117:16:1:151$. Phytoplankton growth is limited by light and nutrients
(phosphate and nitrate), assuming that the most limiting resource determines the growth rate.
Phytoplankton is grazed by zooplankton as described a Holling Type III function with a
quadratic dependence on phytoplankton biomass. The model assumes that a fixed fraction
(15%) of egestion, zooplankton mortality, and phytoplankton loss is released as DOP, and the
rest becomes detritus. Attenuation of detritus (POP) down the water column is described via
the Martin Curve. A fraction of detritus that reaches the seafloor is buried instantaneously,
and the non-buried fraction is resuspended back into the water column. The global river
runoff equivalent to the annual flux of total organic P buried in the previous year is
resupplied to the surface box to close the phosphorus budget (Kriest & Oschlies, 2013). The
key biogeochemical parameters, including the Martin *b*, were objectively calibrated
specifically for the ECCO transport matrix field to match observed PO_4, O_2, and NO_3 (Kriest
et al., 2020; Figure S1).

2.2.2 Flexible C:P dynamics
This study added four new state variables related to organic carbon: phytoplankton carbon,
zooplankton carbon, DOC, and detritus carbon (which we refer to as POC) to simulate the
variable C:P ratio of organic matter. Phytoplankton P:C ratio in production layers is modeled
using the power-law formulation as a function of ambient temperature and PO_4 (Tanioka &
Matsumoto, 2017, 2020):

176 $$[P:C]_{PHY} = [P:C]_{PHY,ref} \cdot \left(\frac{[PO_4]}{[PO_4]_0}\right)^{s_{PO_4}^{P:C}} \cdot \left(\frac{T}{T_0}\right)^{s_T^{P:C}}$$ (1)

177

178 The exponents are the sensitivity factors determined by a meta-analysis (Tanioka and
179 Matsumoto, 2020), and the subscript "0" indicates the reference environmental values, where
180 at these values, P:C equals the reference P:C (i.e., $[P:C]_{PHY,ref}$ = Redfield Ratio = 1:117).
181 The complete list of parameters used in the model is provided in Table S5.

182

183 Zooplankton P:C ratio is flexible and computed as a function of phytoplankton P:C in a
184 power-law formulation:

185

186 $$[P:C]_{zoo} = [P:C]_{zoo,ref}^{1-H}[P:C]_{PHY}^{H}$$ (2)

187

188 where H is the homeostasis parameter, which takes a value of 0 when zooplankton P:C is
189 completely homeostatic and a value of 1 when $[P:C]_{zoo}$ is directly proportional to $[P:C]_{PHY}$.
190 In our study, we use H of 0.08 based on the meta-analysis by Persson et al. (2010) and assign
191 the reference P:C of zooplankton, $[P:C]_{zoo,ref}$, equal to the Redfield ratio of 1:117. For
192 zooplankton to maintain homeostatic C:P and cancel the mismatch between C:P of prey and
193 themselves, zooplankton egests excess C into the environment as a new POC. Although
194 studies suggest that 10-30% of POC ingested by zooplankton is released as DOC (Steinberg
195 & Landry, 2017), we assume here for simplicity that all of the egested carbon goes to the
196 POC pool.

197

198 For this study, we further assume that phytoplankton are always more C-rich than
199 zooplankton (i.e., $[P:C]_{PHY} < [P:C]_{zoo}$) by setting hard-bound maximum $[P:C]_{PHY}$ to
200 equal 1:117. With this simplification, zooplankton will only release excess C but not excess P.
201 This ensures that the stoichiometry regulation of zooplankton will not affect values of
202 inorganic nutrients and allows a fair comparison of model results across different sensitivity
203 runs mentioned later. Some laboratory studies support our assumption that phytoplankton are
204 more carbon-rich than zooplankton even under P-sufficient conditions (e.g., Boersma et al.,
205 2009), and we believe that release of excess P by zooplankton occurs much less frequently
206 than the release of excess C in most of the open ocean.

207

208 Kinetic parameters such as rate constants (λ) for remineralization for various source-minus-
209 sink terms of POC and DOC are identical to those of POP and DOP, respectively. In the
210 default run, the same Martin parameter (b = 1.46) is assigned to both POC and POP so that
211 both elements have the same remineralization length scale and there is no preferential
212 remineralization of one over the other. This default Martin b value of 1.46 is specifically

213 derived for MOPS by Kriest et al. (2020) to give the best fit toward hydrographic and satellite
214 observations and is different from the original Martin b parameter of 0.86 (J. H. Martin et al.,
215 1987). A full description of source-minus-sink terms of the ocean biogeochemistry model is
216 given in Text S1.
217
218 **2.2.3 Numerical experimental setup**
219 We initialized MOPS for 3000 years under the constant climate scenario with fixed
220 atmospheric pCO_2 at 280 ppm using monthly mean TMs, wind speed, temperature, salinity,
221 and spatially variable P:C uptake ratios for phytoplankton and zooplankton following
222 Equations (1) and (2) (Figure 1a, Figure S2). Following the 3000-year spin-up run, at which
223 point the model has reached a steady state, we conducted sensitivity experiments to evaluate
224 the response of the soft tissue pump to change in the C:P ratio of sinking POM. We
225 systematically varied the Martin b parameter for POC (b_C) between 0.75 and 1.75 while
226 keeping the Martin parameter for POP (b_P) constant at 1.46 to allow preferential
227 remineralization of POP and POC over one another. This parameter range of b_C, while
228 keeping b_P constant and applied to our model, brackets the global observed range in C:P flux
229 at depth (Figure 1b). When b_C is smaller than the fixed b_P of 1.46, POP is preferentially
230 remineralized over POC, and vice versa when b_C is greater than 1.46. Keeping the POP
231 attenuation profile constant and not considering CO_2 radiative feedback across sensitivity
232 runs ensures that the concentrations of all non-carbon tracers are identical in each sensitivity
233 run. Oxygen demand during aerobic remineralization is computed from remineralization of
234 organic phosphorus and not from organic carbon, with fixed stoichiometry; thus, oxygen
235 utilization is kept identical in each run. This way, we can effectively isolate the effect of C:P
236 on the strength of soft-tissue carbon pump without changing oxygen concentration and
237 preformed and regenerated phosphate concentrations.
238
239 Following a 3000-year spin-up run, allowing all the chemical tracers to reach steady-state
240 concentration, we conducted sensitivity runs with varying b_C for 1000 years to allow carbon-
241 based tracers to reach new equilibrium states. CO_2 drift in the control run after 1000 years
242 was -2.2 ppm, so we corrected for that deviation in each sensitivity run. The total amount of
243 carbon in the ocean-atmosphere system remains constant as C:P of river supply and burial are
244 fixed at 117, and phosphate inventory is steady. MOPS assumes OCMIP-type, gas exchange
245 protocol with piston velocity and saturation derived from a monthly mean wind speed,
246 salinity, and temperature derived from the MIT ECCO Ocean model and interpolated linearly
247 onto the current time step (Kriest & Oschlies, 2015). In sensitivity experiments, we applied
248 an infinitely fast gas exchange where surface ocean pCO_2 at each time step is in equilibrium
249 with atmospheric pCO_2 to remove the effects of air-sea disequilibrium and reduce the time it
250 takes for the system to reach a new equilibrium. In addition, alkalinity is kept spatially

251 uniform in all the sensitivity runs. These assumptions are essential for isolating the effects of
252 the soft-tissue pump on atmospheric pCO_2 without complications caused by disequilibrium
253 (Cliff et al., 2021; Khatiwala et al., 2019) and comparing model results with the theoretical
254 predictions.

255 **3. Results**

256 **3.1 Depth-dependent change in POC:POP flux ratio**
257 Our new data compilation indicates that the C:P ratio of sinking POM in the twilight zone
258 (100 – 1000 m) is generally higher than the regionally averaged C:P of suspended POM in
259 the top 300 m in the overlying water column (Figure 1b). Observed C:P flux ratios in the
260 twilight zone range between 83:1 and 500:1 with the global median of 294:1 (Table S2). This
261 is approximately a factor of two greater than the global weighted mean C:P of suspended
262 matter of 146:1 in the top 50 m (Martiny et al., 2013). Regionally, the tropical Atlantic
263 exhibits the highest C:P flux ratio of 334:1 in the twilight zone, followed by the tropical
264 Pacific (C:P = 318:1) and the Subtropical North Atlantic (C:P = 279:1). The Subpolar North
265 Pacific region shows the lowest C:P flux ratio of 142:1 but is still higher than the mean
266 surface suspended particle C:P of 94:1 in that region (Martiny et al., 2013, 2014). Two-way
267 ANOVA shows that the geographic regions and the depth at which the samples are collected
268 significantly affect the C:P flux ratio ($p < 0.05$; Table S3). C:P export flux ratio in the
269 twilight zone measured by surface-tethered sediment traps are significantly elevated
270 compared to C:P flux ratio measured in the deep ocean (> 1000 m) by moored sediment traps
271 ($p < 0.05$). Our new data compilation confirms previous findings that the mean C:P flux ratio
272 of sinking organic matter in the twilight zone is generally higher than the C:P of suspended
273 POM (Knauer et al., 1979; Menzel & Ryther, 1964).
274
275 In addition to the global compilation, POM dynamics in the BATS ocean time-series provide
276 continuous sedimentary POC and PP fluxes in the top mesopelagic depths (150 ~ 300 m)
277 from 2006 to 2019. Median Martin b is significantly higher for PP ($b_P = 1.28$) compared to
278 POC ($b_C = 0.98$), which indicates a shallower remineralization profile of PP over POC
279 (Figure 2b, Table S4). There were no temporal shifts in the magnitude of Martin b for PP and
280 POC between 2006 and 2019, but the systematic difference in Martin b for PP and POC at
281 BATS is persistent over time (Figure 2a), indicating that preferential remineralization of PP
282 over POC is a prevalent feature in the subtropical region.
283
284 **3.2 Effects of variable C:P export stoichiometry on pCO_2: Theory and Model Results**
285 Following the first-principle argument (Ito & Follows, 2005; Marinov, Follows, et al., 2008;
286 Marinov, Gnanadesikan, et al., 2008), the total ocean carbon storage due to soft-tissue pump

287 (OCS_{soft}) can be determined by the remineralized PO_4 inventory ($\overline{PO_{4remin}}$) scaled by a
288 global mean C:P ratio of remineralization ($r_{C:P}$):

289

290 $OCS_{soft} = r_{C:P} \cdot \overline{PO_{4remin}} \cdot V_{oc}$
291 $\quad\quad\quad = r_{C:P} \cdot (\overline{PO_4} - \overline{PO_{4pref}}) \cdot V_{oc}$ $\hphantom{xxxxxxxxxxxxxxxxxxxxxxxxx}$ (3)

292

293 where V_{OC} is the ocean volume, and $\overline{PO_4}$ (= 2.14 mmol m^{-3}) and $\overline{PO_{4pref}}$ (= 1.09 mmol m^{-3})
294 are global volume averages for total PO_4 and preformed PO_4, respectively obtained from our
295 MOPS-ECCO model simulation at steady state. Preformed PO_4 in the ocean interior in model
296 simulations is computed from AOU and fixed -O_2:P of 151.1. Our modeled mean PO_4
297 compares well with observed global mean PO_4 of 2.26 mmol m^{-3}, and mean observed
298 preformed PO_4 concentrations of 2.2 mmol m^{-3} and 0.8 mmol m^{-3} for Antarctic Bottom Water
299 (AABW) and North Atlantic Deepwater (NADW), respectively (Duteil et al., 2012).

300

301 Atmospheric pCO_{2a} can be related to global mean C:P assuming constant phosphate
302 inventory, total buffered carbon in the ocean ($C_{buffered}$), and pCO_2 when OCS_{soft} is zero ($c_1 =$
303 651 ppm):

304

305 $pCO_{2a} \cong c_1 \cdot e^{-\frac{OCS_{soft}}{C_{buffered}}} = c_1 \cdot e^{-\frac{r_{C:P} \cdot (\overline{PO_4} - \overline{PO_{4pref}}) \cdot V_{oc}}{C_{buffered}}}$ $\hphantom{xxxxxxxxx}$ (4)

306

307 The definition of "buffered carbon" ($C_{buffered}$) follows that of previous studies (Goodwin et
308 al., 2007; Marinov, Follows, et al., 2008; Marinov, Gnanadesikan, et al., 2008):

309

$\quad$ $C_{buffered} = M_a \cdot pCO_{2a} + V_{oc} \cdot \overline{DIC_{eq}}/R \cong \text{constant}$

310

311 where M_a is the mass of the atmosphere, R is the Revelle buffer factor, and $\overline{DIC_{eq}}$ is the
312 globally averaged surface equilibrium DIC (Table S6).

313

314 We posit that the global mean C:P of remineralization ($r_{C:P}$) can be predicted as the ratio
315 between the globally integrated flux of POC and POP in the twilight zone:

316

317 $r_{C:P} \cong \dfrac{\int_{z_0}^{z'} F_{C,0}\left(\frac{z}{z_0}\right)^{-b_C} dz}{\int_{z_0}^{z'} F_{P,0}\left(\frac{z}{z_0}\right)^{-b_P} dz} = r_{C:P}(z_0) \cdot \dfrac{\int_{z_0}^{z'}\left(\frac{z}{z_0}\right)^{-b_C} dz}{\int_{z_0}^{z'}\left(\frac{z}{z_0}\right)^{-b_P} dz}$ $\hphantom{xxxx}$ (5)

318

319   where $r_{C:P}(z_0)$ is the global mean C:P of NPP in the euphotic zone at depth z_0; b_P and b_C are
320   Martin's b exponent for POP and POC, respectively, and z' is the bottom of the depth of the
321   twilight zone. For theoretical prediction of the global mean $r_{C:P}$ from Equation (5), we used
322   fixed surface reference depth z_0 of 100 m and tested different mesopelagic depth horizons z'
323   (250, 1000, and 2000 m). We compared true OCS_{soft} and $pCO2_a$ from the model output with
324   the theoretical predictions based on Equations (3) – (5) and assessed how well $r_{C:P}$ could be
325   estimated from the Martin b parameters alone.
326
327   Figure 3a illustrates the relationship between $r_{C:P}$ and the strength of the soft-tissue pump
328   measured by the total ocean carbon storage due to soft-tissue pump, OCS_{soft}, at steady-state.
329   Each steady state model results with different values of b_C are shown as individual points
330   with different colors. Theoretical predictions with different mesopelagic depth horizons z' are
331   shown with lines, and the depth selection z' of 1000 m best matches the model results. A
332   good agreement between the model result and theory gives us confidence that much of the
333   change in $r_{C:P}$ can be explained by preferential remineralization of POP over POC occurring
334   in the twilight zone (between 100 - 1000 m) and not in the epipelagic or bathypelagic regions
335   of the ocean.
336
337   Our model results suggest that $r_{C:P}$ can change the strength of ocean soft-tissue pump and
338   atmospheric CO_2 drawdown in two ways. First is via a change in the surface C:P ratio,
339    $r_{C:P}(z_0)$, and this effect can be visualized by comparing the model output with fixed C:P
340   ("Redfield") and the "Default ($b_c = b_p$)" run with variable C:P at the surface but no
341   preferential remineralization at depth. Incorporating variable surface C:P can increase carbon
342   export at 100 m by 3.0 PgC yr^{-1} compared to the Redfield run and increase the total carbon
343   storage by 422 PgC or 21% (Table S6). It is important to note that this mechanism implicitly
344   assumes that small cells are exported more efficiently if the increase in C:P of phytoplankton
345   is tied to the reduction in the weighted size of the phytoplankton.
346
347   The second effect for strengthening soft-tissue pump is via an increase in the remineralization
348   length scale of POC by reducing b_C relative to b_P. The global mean C:P remineralization ratio,
349    $r_{C:P}$, increases from 142 in the default run with no preferential remineralization to as high as
350   309 when b_C is roughly halved from 1.46 to 0.75. Halving b_C in the model decreases pCO_2 by
351   ~180 ppm from 305 ppm to 128 ppm and more than doubles the carbon storage by the soft-
352   tissue pump. There is a range of 100 ppm given the large spread in b_C required to explain the
353   observed C:P of POM flux (Figure 1), and the real-world range of pCO_2 remains difficult to
354   be constrained in the current study. However, our sensitivity model runs indicate the potential
355   of particle flux stoichiometry to significantly perturb the global carbon cycle.
356

357 An increase in the particle $r_{C:P}$ in the twilight zone and the subsequent strengthening of soft-
358 tissue carbon pump leads to reduction of DIC in the surface and more DIC sequestration in
359 the mid to deep ocean (Figure S3). In the "Default" model run with variable C:P at the
360 surface but with no change in C:P at depth, ΔDIC from the Redfield run is mainly limited in
361 the top 1000 m, and the carbon sequestration signal does not penetrate to the deep ocean
362 (Figure S3c, d). However, when we allow the depth-dependent increase in POC:POP flux via
363 assigning the lower value of b_C, the signal of variable stoichiometry can potentially readily
364 reach the deep ocean. The largest DIC increase occurs in the deep North Pacific Ocean,
365 reflecting the greater accumulation of respired carbon along the deep branch of the
366 overturning circulation (Figure S3e, f). Accumulation of DIC in the deep Pacific is
367 accompanied by a considerable reduction of DIC concentration in the surface ocean and
368 NADW, which is indicative of the subduction of the DIC deplete surface water transported
369 poleward.
370
371 **4. Discussion and Outlook**
372 Our data compilation suggests that, on average, particulate organic carbon has a longer
373 remineralization length scale than particulate phosphorus, thus leading to an increased C:P
374 export flux ratio with depth in the twilight zone. However, we do not currently have a good
375 understanding of the mechanisms that lead to such stoichiometric variability. Previous studies
376 (Broecker, 1982b, 1982a; Wakeham et al., 1984) speculated that decoupling of POC and POP
377 remineralization could occur in three steps: (1) selective removal of the more labile organic
378 matter fractions during the digestive process of zooplankton, (2) formation of fecal pellets
379 enriched with non-labile organic matter such as fiber, and (3) consolidation of fragmented
380 sloppy feeding material and fecal material into larger sinking particles. When food quality is
381 low (i.e., high C:P of prey), zooplankton retains nutritive elements such as P and N while
382 releasing crude fiber carbon behind as feces leading to high C:P of fecal pellets (Steinberg &
383 Landry, 2017). These mechanisms provide plausible reasons for a larger positive deviation of
384 C:P of sinking POM relative to surface suspended POM in the oligotrophic regions (e.g.,
385 Subtropical North Pacific) compared to more nutrient-rich regions (e.g., Subpolar North
386 Pacific).
387
388 Microbial transformation of sinking particles can further give rise to C:P in the twilight zone
389 if microbes attached to the particles preferentially remineralize P over C (Karl et al., 1996;
390 Taylor et al., 1986). However, the biochemical mechanisms for preferential remineralization
391 of POM by heterotrophic microbes are somewhat more uncertain than dissolved organic
392 matter (DOM) because the biochemical compositions of DOM and POM are quite different
393 (Loh & Bauer, 2000; Paytan et al., 2003). Although preferential removal of different types of
394 particulate organic phosphorus compounds, such as phosphonates relative to phosphoesters,

395 have been observed (Benitez-Nelson et al., 2004), and bacteria are known to have a greater
396 tendency for consuming P than C from their food substrates (Gundersen et al., 2002), we do
397 not currently have a good understanding of mechanisms how bacteria attached to sinking
398 POM can preferentially remineralize P over C (Benitez-Nelson, 2000).
399
400 Physical mechanisms such as abiotic particle fragmentation that physically removes P may
401 also increase the C:P flux ratio at depth. It has been suggested that the smaller, older
402 refractory particles that have undergone more fragmentation contribute a greater fraction of
403 POM collected in the deeper trap samples because smaller particles generally have a longer
404 residence time in the oceans (Karl et al., 1988; Wakeham et al., 1984). Physical mixing and
405 circulation are also likely to be vital in explaining why C:P flux ratios do not continue to
406 increase indefinitely below the twilight zone. As nutrient concentrations in the deep ocean (>
407 400 m) show that the globally averaged bulk of organic matter remineralization occurs in
408 approximately Redfield ratio (Anderson & Sarmiento, 1994), the physical mechanisms
409 maybe playing critical roles in averaging the signal of elevated POC:POP in the surface and
410 twilight zone from reaching the deep ocean (Shaffer et al., 1999; Weber & Deutsch, 2010).
411
412 Methodological issues related to sediment traps, including hydrodynamic biases, swimmers,
413 and solubilization, prohibit us from making firm quantitative conclusions on the extent of
414 selective remineralization of POP over POC at different oceanographic regions (Buesseler,
415 Antia, et al., 2007). A previous study showed that solubilization of P after being collected in
416 the sediment traps occurs at a much greater extent relative to C and could change the
417 estimation of the stoichiometric C:P ratios of sinking particles (Antia, 2005; Buesseler et al.,
418 2007). However, enhanced remineralization and solubilization of P, relative to C, whether it
419 occurs in the water column or in the sediment trap, support our point that P is more labile
420 than C.
421
422 Here, we showed using a 3D model and theory that C:P variability in the twilight zone can
423 modulate the strength of carbon sequestration by at least 20%. Our result is unique in that
424 redistribution of DIC can occur without a change in the nutrient distribution, and the change
425 in DIC distribution is entirely through the change in particle export stoichiometry. Ocean
426 biogeochemical models are beginning to incorporate flexible C:N:P of phytoplankton (Chien
427 et al., 2020; Kwiatkowski et al., 2018; Matsumoto et al., 2021; Pahlow et al., 2020) but most
428 models do not yet explicitly consider a change in the elemental stoichiometry of POM once it
429 leaves below the euphotic zone. In this regard, other mathematical forms of remineralization
430 profiles such as exponential function (Armstrong et al., 2001; Lauderdale & Cael, 2021;
431 Pavia et al., 2019) to prevent flux stoichiometry from increasing indefinitely with depth. In
432 addition to modeling passive fluxes, models also need to consider active transport of material

via vertically migrating animals and how they change C:N:P flux stoichiometry in the twilight zone (Hannides et al., 2009; Saba et al., 2021; Schiettekatte et al., 2020). As many biogeochemical processes in the ocean twilight zone that govern particle transfer are still enigmatic (Boyd et al., 2019; Robinson et al., 2010), future studies using new technologies such as Underwater Vision Profilers, robots, and autonomous Argo floats could significantly advance our current understanding of particle dynamics in the twilight zone (A. Martin et al., 2020).

Reference:

Anderson, L. A., & Sarmiento, J. L. (1994). Redfield ratios of remineralization determined by nutrient data analysis. *Global Biogeochemical Cycles*, *8*(1), 65–80. https://doi.org/10.1029/93GB03318

Antia, A. N. (2005). Solubilization of particles in sediment traps: revising the stoichiometry of mixed layer export. *Biogeosciences*, *2*(2), 189–204. https://doi.org/10.5194/bg-2-189-2005

Armstrong, R. A., Lee, C., Hedges, J. I., Honjo, S., & Wakeham, S. G. (2001). A new, mechanistic model for organic carbon fluxes in the ocean based on the quantitative association of POC with ballast minerals. *Deep-Sea Research Part II: Topical Studies in Oceanography*, *49*(1–3), 219–236. https://doi.org/10.1016/S0967-0645(01)00101-1

Benitez-Nelson, C. R. (2000). The biogeochemical cycling of phosphorus in marine systems. *Earth-Science Reviews*, *51*(1–4), 109–135. https://doi.org/10.1016/S0012-8252(00)00018-0

Benitez-Nelson, C. R., O'Neill, L., Kolowith, L. C., Pellechia, P., & Thunell, R. (2004). Phosphonates and particulate organic phosphorus cycling in an anoxic marine basin. *Limnology and Oceanography*, *49*(5), 1593–1604. https://doi.org/10.4319/lo.2004.49.5.1593

Benitez-Nelson, C. R., O'Neill Madden, L. P., Styles, R. M., Thunell, R. C., & Astor, Y. (2007). Inorganic and organic sinking particulate phosphorus fluxes across the oxic/anoxic water column of Cariaco Basin, Venezuela. *Marine Chemistry*, *105*(1–2), 90–100. https://doi.org/10.1016/j.marchem.2007.01.007

474   Boersma, M., Becker, C., Malzahn, A. M., & Vernooij, S. (2009). Food chain effects of nutrient limitation in
475   primary producers. *Marine and Freshwater Research*, *60*(10), 983–989. https://doi.org/10.1071/MF08240
476   Boyd, P. W., Claustre, H., Levy, M., Siegel, D. A., & Weber, T. S. (2019). Multi-faceted particle pumps drive
477   carbon sequestration in the ocean. *Nature*, *568*(7752), 327–335. https://doi.org/10.1038/s41586-019-1098-
478   2
479   Broecker, W. S. (1982a). Glacial to interglacial changes in ocean chemistry. *Progress in Oceanography*, *11*(2),
480   151–197. https://doi.org/10.1016/0079-6611(82)90007-6
481   Broecker, W. S. (1982b). Ocean chemistry during glacial time. *Geochimica et Cosmochimica Acta*, *46*(10),
482   1689–1705. https://doi.org/10.1016/0016-7037(82)90110-7
483   Buesseler, K. O., Antia, A. N., Chen, M., Fowler, S. W., Gardner, W. D., Gustafsson, O., et al. (2007). An
484   assessment of the use of sediment traps for estimating upper ocean particle fluxes. *Journal of Marine*
485   *Research*, *65*(3), 345–416. https://doi.org/10.1357/002224007781567621
486   Chien, C.-T., Pahlow, M., Schartau, M., & Oschlies, A. (2020). Optimality-based non-Redfield plankton-
487   ecosystem model (OPEM v1.1) in UVic-ESCM 2.9 - Part 2: Sensitivity analysis and model calibration.
488   *Geoscientific Model Development*, *13*(10), 4691–4712. https://doi.org/10.5194/gmd-13-4691-2020
489   Christian, J. R., Lewis, M. R., & Karl, D. M. (1997). Vertical fluxes of carbon, nitrogen, and phosphorus in the
490   North Pacific Subtropical Gyre near Hawaii. *Journal of Geophysical Research: Oceans*, *102*(C7), 15667–
491   15677. https://doi.org/10.1029/97JC00369
492   Cliff, E., Khatiwala, S., & Schmittner, A. (2021). Glacial deep ocean deoxygenation driven by biologically
493   mediated air–sea disequilibrium. *Nature Geoscience*, *14*(1), 43–50. https://doi.org/10.1038/s41561-020-
494   00667-z
495   Duteil, O., Koeve, W., Oschlies, A., Aumont, O., Bianchi, D., Bopp, L., et al. (2012). Preformed and
496   regenerated phosphate in ocean general circulation models: can right total concentrations be wrong?
497   *Biogeosciences*, *9*(5), 1797–1807. https://doi.org/10.5194/bg-9-1797-2012
498   Engel, A., Wagner, H., Le Moigne, F. A. C., & Wilson, S. T. (2017). Particle export fluxes to the oxygen
499   minimum zone of the eastern tropical North Atlantic. *Biogeosciences*, *14*(7), 1825–1838.
500   https://doi.org/10.5194/bg-14-1825-2017
501   Faul, K. L., Paytan, A., & Delaney, M. L. (2005). Phosphorus distribution in sinking oceanic particulate matter.
502   *Marine Chemistry*, *97*(3–4), 307–333. https://doi.org/10.1016/j.marchem.2005.04.002
503   Garcia, H., Weathers, K. W., Paver, C. R., Smolyar, I., Boyer, T. P., Locarnini, R. A., et al. (2018). World
504   Ocean Atlas 2018. Volume 4: Dissolved Inorganic Nutrients (phosphate, nitrate and nitrate+nitrite,
505   silicate). In A. Mishonov (Ed.), *NOAA Atlas NESDIS 84* (Vol. 84, p. 35).
506   Goodwin, P., Williams, R. G., Follows, M. J., & Dutkiewicz, S. (2007). Ocean-atmosphere partitioning of
507   anthropogenic carbon dioxide on centennial timescales. *Global Biogeochemical Cycles*, *21*(1), 1–10.
508   https://doi.org/10.1029/2006GB002810
509   Grabowski, E., Letelier, R. M., Laws, E. A., & Karl, D. M. (2019). Coupling carbon and energy fluxes in the
510   North Pacific Subtropical Gyre. *Nature Communications*, *10*(1), 1895. https://doi.org/10.1038/s41467-
511   019-09772-z
512   Gundersen, K., Heldal, M., Norland, S., Purdie, D. A., & Knap, A. H. (2002). Elemental C, N, and P cell content
513   of individual bacteria collected at the Bermuda Atlantic Time-series Study (BATS) site. *Limnology and*
514   *Oceanography*, *47*(5), 1525–1530. https://doi.org/10.4319/lo.2002.47.5.1525
515   Hannides, C. C. S., Landry, M. R., Benitez-Nelson, C. R., Styles, R. M., Montoya, J. P., & Karl, D. M. (2009).
516   Export stoichiometry and migrant-mediated flux of phosphorus in the North Pacific Subtropical Gyre.
517   *Deep-Sea Research Part I: Oceanographic Research Papers*, *56*(1), 73–88.
518   https://doi.org/10.1016/j.dsr.2008.08.003
519   Ito, T., & Follows, M. J. (2005). Preformed phosphate, soft tissue pump and atmospheric CO_2. *Journal of*

Marine Research, *63*(4), 813–839. https://doi.org/10.1357/0022240054663231

Karl, D. M., Knauer, G. A., & Martin, J. H. (1988). Downward flux of particulate organic matter in the ocean: a particle decomposition paradox. *Nature*, *332*(6163), 438–441. https://doi.org/10.1038/332438a0

Karl, D. M., Christian, J. R., Dore, J. E., Hebel, D. V., Letelier, R. M., Tupas, L. M., & Winn, C. D. (1996). Seasonal and interannual variability in primary production and particle flux at Station ALOHA. *Deep Sea Research Part II: Topical Studies in Oceanography*, *43*(2–3), 539–568. https://doi.org/10.1016/0967-0645(96)00002-1

Karl, D. M., Church, M. J., Dore, J. E., Letelier, R. M., & Mahaffey, C. (2012). Predictable and efficient carbon sequestration in the North Pacific Ocean supported by symbiotic nitrogen fixation. *Proceedings of the National Academy of Sciences of the United States of America*, *109*(6), 1842–1849. https://doi.org/10.1073/pnas.1120312109

Khatiwala, S. (2007). A computational framework for simulation of biogeochemical tracers in the ocean. *Global Biogeochemical Cycles*, *21*(3). https://doi.org/10.1029/2007GB002923

Khatiwala, S., Visbeck, M., & Cane, M. A. (2005). Accelerated simulation of passive tracers in ocean circulation models. *Ocean Modelling*, *9*(1), 51–69. https://doi.org/10.1016/j.ocemod.2004.04.002

Khatiwala, S., Primeau, F. W., & Holzer, M. (2012). Ventilation of the deep ocean constrained with tracer observations and implications for radiocarbon estimates of ideal mean age. *Earth and Planetary Science Letters*, *325–326*, 116–125. https://doi.org/10.1016/j.epsl.2012.01.038

Khatiwala, S., Schmittner, A., & Muglia, J. (2019). Air-sea disequilibrium enhances ocean carbon storage during glacial periods. *Science Advances*, *5*(6), 1–11. https://doi.org/10.1126/sciadv.aaw4981

Knauer, G. A., Martin, J. H., & Bruland, K. W. (1979). Fluxes of particulate carbon, nitrogen, and phosphorus in the upper water column of the northeast Pacific. *Deep Sea Research Part A. Oceanographic Research Papers*, *26*(1), 97–108. https://doi.org/10.1016/0198-0149(79)90089-X

Kriest, I., & Oschlies, A. (2013). Swept under the carpet: Organic matter burial decreases global ocean biogeochemical model sensitivity to remineralization length scale. *Biogeosciences*, *10*(12), 8401–8422. https://doi.org/10.5194/bg-10-8401-2013

Kriest, I., & Oschlies, A. (2015). MOPS-1.0: Towards a model for the regulation of the global oceanic nitrogen budget by marine biogeochemical processes. *Geoscientific Model Development*, *8*(9), 2929–2957. https://doi.org/10.5194/gmd-8-2929-2015

Kriest, I., Kähler, P., Koeve, W., Kvale, K. F., Sauerland, V., & Oschlies, A. (2020). One size fits all? Calibrating an ocean biogeochemistry model for different circulations. *Biogeosciences*, *17*(12), 3057–3082. https://doi.org/10.5194/bg-17-3057-2020

Kwiatkowski, L., Aumont, O., Bopp, L., & Ciais, P. (2018). The Impact of Variable Phytoplankton Stoichiometry on Projections of Primary Production, Food Quality, and Carbon Uptake in the Global Ocean. *Global Biogeochemical Cycles*, *32*(4), 516–528. https://doi.org/10.1002/2017GB005799

Kwon, E. Y., Primeau, F. W., & Sarmiento, J. L. (2009). The impact of remineralization depth on the air-sea carbon balance. *Nature Geoscience*, *2*(9), 630–635. https://doi.org/10.1038/ngeo612

Lamborg, C. H., Buesseler, K. O., Valdes, J., Bertrand, C. H., Bidigare, R., Manganini, S., et al. (2008). The flux of bio- and lithogenic material associated with sinking particles in the mesopelagic "twilight zone" of the northwest and North Central Pacific Ocean. *Deep Sea Research Part II: Topical Studies in Oceanography*, *55*(14–15), 1540–1563. https://doi.org/10.1016/j.dsr2.2008.04.011

Lauderdale, J. M., & Cael, B. B. (2021). Impact of Remineralization Profile Shape on the Air-Sea Carbon Balance. *Geophysical Research Letters*, *48*(7), e2020GL091746. https://doi.org/10.1029/2020GL091746

Loh, A. N., & Bauer, J. E. (2000). Distribution, partitioning and fluxes of dissolved and particulate organic C, N and P in the eastern North Pacific and Southern Oceans. *Deep Sea Research Part I: Oceanographic Research Papers*, *47*(12), 2287–2316. https://doi.org/10.1016/S0967-0637(00)00027-3

566 Lomas, M. W., Burke, A. L., Lomas, D. A., Bell, D. W., Shen, C., Dyhrman, S. T., & Ammerman, J. W. (2010).
567   Sargasso Sea phosphorus biogeochemistry: An important role for dissolved organic phosphorus (DOP).
568   *Biogeosciences*, *7*(2), 695–710. https://doi.org/10.5194/bg-7-695-2010
569 Marinov, I., Follows, M. J., Gnanadesikan, A., Sarmiento, J. L., & Slater, R. D. (2008). How does ocean biology
570   affect atmospheric p CO_2? Theory and models. *Journal of Geophysical Research*, *113*(C7), C07032.
571   https://doi.org/10.1029/2007JC004598
572 Marinov, I., Gnanadesikan, A., Sarmiento, J. L., Toggweiler, J. R., Follows, M., & Mignone, B. K. (2008).
573   Impact of oceanic circulation on biological carbon storage in the ocean and atmospheric p CO_2. *Global
574   Biogeochemical Cycles*, *22*(3), n/a-n/a. https://doi.org/10.1029/2007GB002958
575 Martin, A., Boyd, P. W., Buesseler, K., Cetinic, I., Claustre, H., Giering, S., et al. (2020). The oceans' twilight
576   zone must be studied now, before it is too late. *Nature*, *580*(7801), 26–28. https://doi.org/10.1038/d41586-
577   020-00915-7
578 Martin, J. H., Knauer, G. A., Karl, D. M., & Broenkow, W. W. (1987). VERTEX: carbon cycling in the
579   northeast Pacific. *Deep Sea Research Part A. Oceanographic Research Papers*, *34*(2), 267–285.
580   https://doi.org/10.1016/0198-0149(87)90086-0
581 Martiny, A. C., Pham, C. T. A., Primeau, F. W., Vrugt, J. A., Moore, J. K., Levin, S. A., & Lomas, M. W.
582   (2013). Strong latitudinal patterns in the elemental ratios of marine plankton and organic matter. *Nature
583   Geoscience*, *6*(4), 279–283. https://doi.org/10.1038/ngeo1757
584 Martiny, A. C., Vrugt, J. A., & Lomas, M. W. (2014). Concentrations and ratios of particulate organic carbon,
585   nitrogen, and phosphorus in the global ocean. *Scientific Data*, *1*, 140048.
586   https://doi.org/10.1038/sdata.2014.48
587 Matsumoto, K. (2007). Biology-mediated temperature control on atmospheric pCO2 and ocean biogeochemistry.
588   *Geophysical Research Letters*, *34*(20), 1–5. https://doi.org/10.1029/2007GL031301
589 Matsumoto, K., Tanioka, T., & Zahn, J. (2021). MESMO 3: Flexible phytoplankton stoichiometry and
590   refractory dissolved organic matter. *Geoscientific Model Development*, *14*(4), 2265–2288.
591   https://doi.org/10.5194/gmd-14-2265-2021
592 Menzel, D. W., & Ryther, J. H. (1964). The Composition of Particulate Organic Matter in the Western North
593   Atlantic. *Limnology and Oceanography*, *9*(2), 179–186. https://doi.org/10.4319/lo.1964.9.2.0179
594 Minster, J. F., & Boulahdid, M. (1987). Redfield ratios along isopycnal surfaces-a complementary study. *Deep
595   Sea Research Part A, Oceanographic Research Papers*, *34*(12), 1981–2003. https://doi.org/10.1016/0198-
596   0149(87)90094-X
597 Pahlow, M., Chien, C.-T., Arteaga, L. A., & Oschlies, A. (2020). Optimality-based non-Redfield plankton-
598   ecosystem model (OPEM v1.1) in UVic-ESCM 2.9 - Part 1: Implementation and model behaviour.
599   *Geoscientific Model Development*, *13*(10), 4663–4690. https://doi.org/10.5194/gmd-13-4663-2020
600 Pavia, F. J., Anderson, R. F., Lam, P. J., Cael, B. B., Vivancos, S. M., Fleisher, M. Q., et al. (2019). Shallow
601   particulate organic carbon regeneration in the South Pacific Ocean. *Proceedings of the National Academy
602   of Sciences of the United States of America*, *116*(20), 9753–9758.
603   https://doi.org/10.1073/pnas.1901863116
604 Paytan, A., Cade-Menun, B. J., McLaughlin, K., & Faul, K. L. (2003). Selective phosphorus regeneration of
605   sinking marine particles: evidence from 31P-NMR. *Marine Chemistry*, *82*(1–2), 55–70.
606   https://doi.org/10.1016/S0304-4203(03)00052-5
607 R Core Team. (2021). R: A Language and Environment for Statistical Computing. Vienna, Austria. Retrieved
608   from https://www.r-project.org/
609 Robinson, C., Steinberg, D. K., Anderson, T. R., Arístegui, J., Carlson, C. A., Frost, J. R., et al. (2010).
610   Mesopelagic zone ecology and biogeochemistry – a synthesis. *Deep Sea Research Part II: Topical Studies
611   in Oceanography*, *57*(16), 1504–1518. https://doi.org/10.1016/j.dsr2.2010.02.018

612   Saba, G. K., Burd, A. B., Dunne, J. P., Hernández-León, S., Martin, A. H., Rose, K. A., et al. (2021). Toward a
613   better understanding of fish-based contribution to ocean carbon flux. *Limnology and Oceanography*, *66*(5),
614   1639–1664. https://doi.org/10.1002/lno.11709
615   Sarmiento, J. L., & Toggweiler, J. R. (1984). A new model for the role of the oceans in determining atmospheric
616   PCO2. *Nature*, *308*(5960), 621–624. https://doi.org/10.1038/308621a0
617   Schiettekatte, N. M. D., Barneche, D. R., Villéger, S., Allgeier, J. E., Burkepile, D. E., Brandl, S. J., et al. (2020).
618   Nutrient limitation, bioenergetics and stoichiometry: A new model to predict elemental fluxes mediated by
619   fishes. *Functional Ecology*, *34*(9), 1857–1869. https://doi.org/10.1111/1365-2435.13618
620   Shaffer, G., Bendtsen, J., & Ulloa, O. (1999). Fractionation during remineralization of organic matter in the
621   ocean. *Deep-Sea Research Part I: Oceanographic Research Papers*, *46*(2), 185–204.
622   https://doi.org/10.1016/S0967-0637(98)00061-2
623   Sigman, D. M., & Boyle, E. A. (2000). Glacial/interglacial variations in atmospheric carbon dioxide. *Nature*,
624   *407*(6806), 859–869. https://doi.org/10.1038/35038000
625   Stammer, D., Ueyoshi, K., Köhl, A., Large, W. G., Josey, S. A., & Wunsch, C. (2004). Estimating air-sea fluxes
626   of heat, freshwater, and momentum through global ocean data assimilation. *Journal of Geophysical*
627   *Research C: Oceans*, *109*(5), C05023. https://doi.org/10.1029/2003JC002082
628   Steinberg, D. K., & Landry, M. R. (2017). Zooplankton and the Ocean Carbon Cycle. *Annual Review of Marine*
629   *Science*, (October 2016), 1–32. https://doi.org/10.1146/annurev-marine-010814-015924
630   Tanioka, T., & Matsumoto, K. (2017). Buffering of Ocean Export Production by Flexible Elemental
631   Stoichiometry of Particulate Organic Matter. *Global Biogeochemical Cycles*, *31*(10), 1528–1542.
632   https://doi.org/10.1002/2017GB005670
633   Tanioka, T., & Matsumoto, K. (2020). A meta-analysis on environmental drivers of marine phytoplankton C :
634   N : P. *Biogeosciences*, *17*(11), 2939–2954. https://doi.org/10.5194/bg-17-2939-2020
635   Taylor, G., Karl, D. M., & Pace, M. (1986). Impact of bacteria and zooflagellates on the composition of sinking
636   particles: an in situ experiment. *Marine Ecology Progress Series*, *29*, 141–155.
637   https://doi.org/10.3354/meps029141
638   Teng, Y.-C., Primeau, F. W., Moore, J. K., Lomas, M. W., & Martiny, A. C. (2014). Global-scale variations of
639   the ratios of carbon to phosphorus in exported marine organic matter. *Nature Geoscience*, *7*(12), 895–898.
640   https://doi.org/10.1038/ngeo2303
641   Wakeham, S. G., Lee, C., Farrington, J. W., & Gagosian, R. B. (1984). Biogeochemistry of particulate organic
642   matter in the oceans: results from sediment trap experiments. *Deep Sea Research Part A. Oceanographic*
643   *Research Papers*, *31*(5), 509–528. https://doi.org/10.1016/0198-0149(84)90099-2
644   Weber, T. S., & Deutsch, C. (2010). Ocean nutrient ratios governed by plankton biogeography. *Nature*,
645   *467*(7315), 550–554. https://doi.org/10.1038/nature09403
646
647

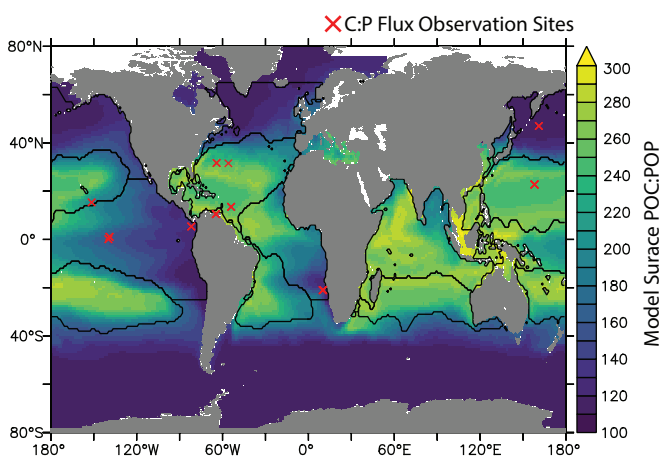648   <u>Figures</u>
649
650   **Figure 1.** Depth profiles of C:P of sinking POM from our new data compilation. (a) Locations of samples
651   collected shown with red crosses superimposed on the modeled C:P of suspended POM at the surface. The
652   boundaries are based on the 0.3 mmol m^{-3} of the annually averaged surface PO_4 concentration. (b) Depth profile
653   of C:P flux ratio of sinking POM (red cross) with C:P of suspended POM in the top 300 m (blue circle; Martiny
654   et al., 2013). C:P flux ratios from a 3D model with different values of b_C (Martin b of POC) are shown with
655   black dotted lines. Only the values between 100 and 2000 m are shown here.

656   **Figure 2.** Martin b estimated from particulate sedimentary flux profiles at BATS. (a) Time-series of the Martin
657   b parameters from 2006 to 2019 for Particulate Phosphorus, PP (b_P, red) and Particulate Organic Carbon, POC
658   (b_C, blue). Smooth lines are Locally Weighted Least Squares Regression. (b) Violin plot for average Martin b
659   values at BATS from 2006 to 2019. The whiskers of the box plot cover 95% confidence interval, and the box
660   shows 25%, 50%, and 75% percentiles. The median values of b_P and b_C are 1.28 and 0.98, respectively.

661
662   **Figure 3.** Comparing model and theoretical prediction on the influence of $r_{C:P}$ on ocean carbon storage at
663   steady state. The relationship between $r_{C:P}$ and (a) ocean carbon storage due to soft-tissue pump and (b)
664   atmospheric CO_2. In both panels, model results are shown with dots, and theoretical predictions with
665   different twilight zone depth range z' are shown with black lines. The color for plots indicates different
666   Martin b parameters for POC used in the simulations. Also shown are threshold OCS_{soft} and pCO_2 when
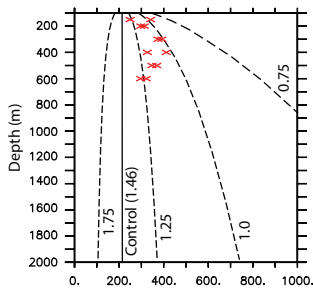667   the entire phosphate is in the regenerated form under fixed $r_{C:P}$ of 117.
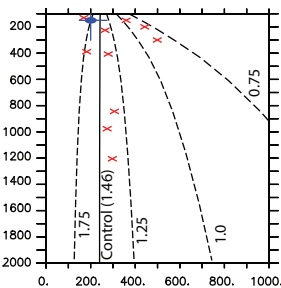
668

Figure 1.
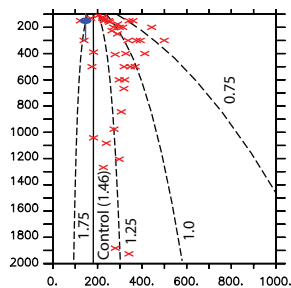
(A) C:P Flux Observation Sites
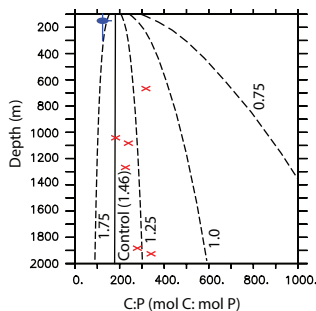
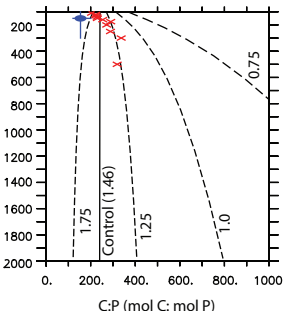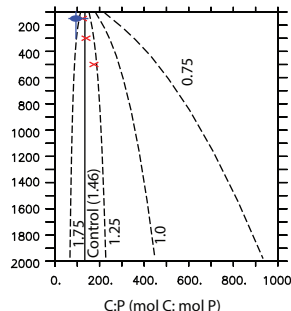(B) Tropical Atlantic | Subtropical North Atlantic | Global

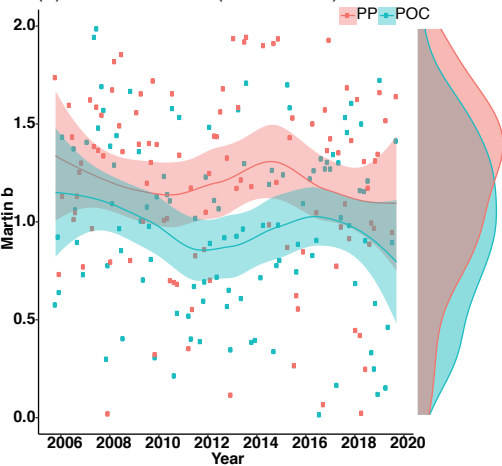Tropical Pacific | Subtropical North Pacific | Subpolar North Pacific

C:P of Suspended POM (measured)   ✕ C:P of Sinking POM Flux (measured)   —— C:P of Sinking POM Flux (modeled, varying b_c)

Figure 2.

(A) Martin b at BATS (150 ~ 300 m)

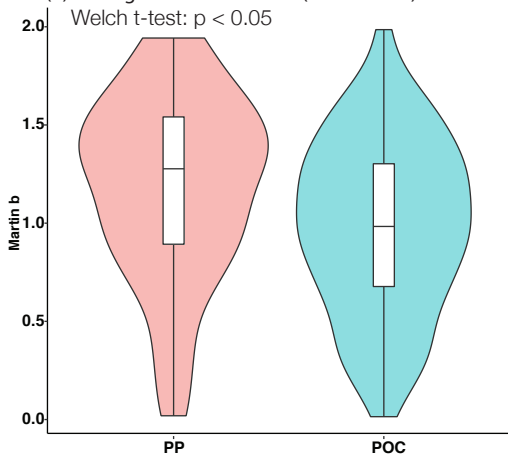**(B)** Average Martin b at BATS (2006 - 2019)
Welch t-test: $p < 0.05$

Figure 3.